ADVANCED MATERIALS
www.advmat.de

Tailoring the Performances of Lead Halide Perovskite Devices with Electron-Beam Irradiation

Ningbo Yi, Shuai Wang, Zonghui Duan, Kaiyang Wang, Qinghai Song, and Shumin Xiao**

Lead halide perovskites are intensively studied in past few years due to their potential applications in optoelectronic devices such as solar cells, photodetectors, light-emitting diodes (LED), and lasers. In addition to the rapid developments in material synthesis and device fabrication, it is also very interesting to postsynthetically control the optical properties with external irradiations. Here, the influences of very low energy (10–20 keV) electron beam of standard electron beam lithography are experimentally explored on the properties of lead halide perovskites. It is confirmed that the radiolysis process also happens and it can selectively change the photoluminescence, enabling the direct formation of nanolaser array, microsized light emitter array, and micropictures with an electron beam writer. Interestingly, it is found that discontinuous metallic lead layers are formed on the top and bottom surfaces of perovskite microplate during the radiolysis process, which can act as carrier conducting layers and significantly increase the photocurrent of perovskite photodetector by a factor of 217%. By using the electron beam with low energy to modify the perovskite, this method promises to shape the emission patterns for micro-LED with well-preserved optical properties and improves the photocurrent of photodetector.

Organic–inorganic lead halide perovskites such as $APbX_3$ (with A = CH_3NH_3/NH_2CH = NH_2, and X = Cl/Br/I)) have been intensively studied due to their wide applications ranging from solar cells to photodetectors, light-emitting diodes (LED), and lasers.[1–8] Owing to its high external quantum efficiency, wide absorption spectrum, low trap-state density, and long carrier diffusion length, the power conversion efficiency of perovskite solar cell have been improved from 3.8% to more than 22.1% within a few years.[9,10] Tailoring the stoichiometry of lead halide perovskite, the corresponding emission and absorption bandedge can be widely tuned from blue light to near infrared.[11,12] Meanwhile, the absorptivity of halide perovskites is ten times higher than that of organic dyes, making them suitable for applications in high-performance photodetectors.[13,14] In past few years, perovskite photodetector with detectivity of 10^{14} Jones has been experimentally realized on FTO (fluorine doped tin oxide) rigid substrate.[15] Meanwhile, perovskite films, bulk crystals, and nanowire-based photodetectors have also been demonstrated. Very recently, with the rapid developments in 2D perovskite sheets, the performances of lead halide perovskite photodetectors have been further improved by orders of magnitude.[16–19]

Associated with the advances of perovskite optoelectronic devices, tailoring the properties of lead halide perovskites with surface passivation or other techniques has also attracted considerable research attention. The optoelectronic properties such as photoluminescence (PL), electroluminescence, and photoconductivity are found to rise slowly over time under light illumination or current flow.[20–24] In 2016, Zhang et al. have observed the enhancement in photoluminescence by exposing lead halide perovskite to chlorine ions via an inductively coupled plasma reactive ion etching process.[25] Following the recent discovery of deQuilettes et al., these changes can be attributed to the halide migration that reduces the trap states and gives homogeneous stoichiometries.[26] Associated with above improvements, electron beam irradiation has also been applied to tailor the characteristics of lead halide perovskites. Recent transmission electron microscope (TEM) studies have consistently reported the rapid degradation of lead halide perovskites under electron beam irradiation.[27] Several groups have clearly observed the formation of nanometer sized high contrast nanoparticles within TEM and scanning TEM images.[28–31] Up to now, while several techniques have been developed to minimize the sample alternations and to achieve very high resolution TEM image, it has been widely accepted that the electron beam irradiation can significantly degrade the performances of lead halide perovskite devices.[26–31] The possibilities of applying electron beam irradiation, especially the electron beam with very low energy, to tailor and even to improve the perovskite devices have not been well explored. Here we experimentally

Dr. N. B. Yi, Dr. S. Wang, Dr. Z. H. Duan, Dr. K. Y. Wang, Prof. Q. H. Song, Prof. S. M. Xiao
State Key Laboratory on Tunable Laser Technology
Ministry of Industry and Information Technology
Key Lab of Micro-Nano Optoelectronic Information System
Shenzhen Graduate School
Harbin Institute of Technology
Shenzhen 518055, China
E-mail: qinghai.song@hit.edu.cn; shumin.xiao@hit.edu.cn
Prof. Q. H. Song, Prof. S. M. Xiao
Collaborative Innovation Center of Extreme Optics
Shanxi University
Taiyuan 030006, China

DOI: 10.1002/adma.201701636

studied the influences of very low energy (10–20 keV) electron beam of standard electron beam lithography on the properties of lead halide perovskites. We confirm that the radiolysis process also happens and it can selectively change the photoluminescence, enabling the direct formation of nanolaser array, microsized light emitter array, and micropictures with an electron beam writer. Interestingly, we find that a partially continuous Pb^0 layers have been formed on the top and bottom surfaces of perovskite microplate, which can act as carrier conducting layers and significantly increase the photocurrent of perovskite photodetector by a factor of 217%.

When lead halide perovskite is illuminated under electron beam with an incident electron energy of tens or hundreds of kiloelectronvolt (keV), there are two main electron-specimen interactions that are known as knock-on damage and radiolysis.[27,32] In general, knock-on damage is dominant at high energy and induces irreversible displacements of nucleus. The radiolysis (ionization damage) involves inelastic scattering process and happens at low energy (≈80 keV in TEM). According to the recent report of Dang et al., the radiolysis is the major mechanism of damage in lead halide perovskite.[27] The low energy electrons stimulate the desorption of a small fraction of bromine atoms and reduce some Pb^{2+} ions to Pb^0. In principle, due to the weaker bonds between edge atoms and surrounding lattice, the electron beam irradiation usually induces structural changes at the surfaces and corners of lead halide perovskites. Compared with the typical semiconductor, the Pb^0 can effectively absorb the photogenerated electrons. In this sense, if a similar radiolysis process happens under very low energy electron beam irradiation, the typical electron beam lithography process has the possibility of directly tailoring or improving the performances of perovskite microlasers or photodetectors.

Based on above analysis, we have experimentally synthesized $CH_3NH_3PbBr_3$ perovskite microplates and studied their changes in optical properties under electron beam irradiation. The $CH_3NH_3PbBr_3$ perovskite microplates were synthesized with the solution processed one-step precipitation method. Basically, the $CH_3NH_3PbBr_3$ precursor was prepared by dissolving $PbBr_2$ and CH_3NH_3Br with a 1:1 molar ratio in *N,N*-dimethylsulfoxide to give a concentration of 0.1 M, followed by a 4 h stirring at 60 °C. The indium tin oxide (ITO) glasses were cleaned by sonication in acetone, isopropanol, and deionized water for 15 min, respectively. Then the $CH_3NH_3PbBr_3$ precursor was drop casted on to the ITO glass, which was located in atmosphere of dichloromethane in a beaker. The beaker was sealed with tetrafluoroethylene films. After a reaction time of ≈24 h, the perovskite microplates with relatively large dimensions have been formed on the ITO glass. **Figure 1**a shows one synthesized perovskite microplate. Its width and length are 30 and 200 μm, respectively. The thickness of the microplate is around 1100 nm (see the inset in Figure 1a). The black line and black dots in Figure 1b are the corresponding absorption and photoluminescence spectra (see the experimental details in Supporting Information). Consistent with the previous reports, a bandedge and a photoluminescence peak at round 550 nm can be clearly seen.

Then the microplate was placed into an electron beam writer (Raith, E-line). The region-2 in Figure 1a was selectively exposed to electron beam with a dose of 150 μC cm^{-2} under a voltage of 20 kV, whereas region-1 was well kept at its original form. Figure 1a and Figure S1 (Supporting Information) illustrate the fluorescent image when the sample was optically excited by a blue laser (450 nm). The photoluminescence of region-2 is much weaker in the fluorescent microscope image. The emission spectrum was plotted as red dots in Figure 1b. Compared with the emission of pristine perovskite, the intensity was reduced by about an order of magnitude after electron beam irradiation. The red line in Figure 1b is the corresponding absorption spectrum. While the bandedge keeps at the same wavelength, the total absorption decreased to about 55%. The decay times of lead halide perovskites have also been studied and shown in Figure 1c and Figure S2 and Table S1 (Supporting Information). For the original $CH_3NH_3PbBr_3$ perovskite, the fast components give a lifetime around 4 ns, and the slow components give a lifetime around 18 ns. Once the sample was radiated by electron beam, the lifetimes drastically reduced to ≈1.58 and ≈4.45 ns, respectively.

To further explore the interaction between electron beam and the $CH_3NH_3PbBr_3$ perovskite, we have systematically changed the dose of electron beam and studied the corresponding photoluminescence of $CH_3NH_3PbBr_3$ perovskite. All the results are summarized in **Figure 2**. From the region-1 to region-7 on the same perovskite microplate (see Figure 2a), the electron beam dose increases from 0, 15, 30, 45, 60, 75 to 90 μC cm^{-2}. The spectra in Figure 2b show that the emission intensity reduces rapidly with the increase of irradiation dose. The inset in Figure 2b shows the dependence of integrated output intensity on the dose of electron beam. While higher dose always relates to smaller photoluminescence intensity, the smallest dose (15 μC cm^{-2}) can still reduce the output about 40%. All of the experiment results in Figures 1 and 2 are consistent and clearly indicate the degradation of photoluminescence from lead halide perovskites under electron beam irradiation.

As the energy of electron beam in this research is much lower than the previous reports (≥80 keV), it is necessary to carefully consider the underlying mechanism of the degradation in photoluminescence.[27] The Energy Dispersive Spectrometer (EDS) measurement was first carried to analyze the elements in the lead halide perovskites in Figure S3 (Supporting Information). Before the electron beam irradiation, the Br/Pb ratio is about 75.91/24.09, which agrees well with a $PbBr_3$ stoichiometry. After the perovskite was irradiated by an electron beam, the Br/Pb ratio is around 75.85/23.15. Here the dose is 150 μC cm^{-2} and the accelerating voltage is 10 kV. The detail experiments show that Br/Pb ratio is almost independent on the dose of electron beam (see Figure S4 in the Supporting Information). Even the sample was damaged by the electron beam, the measured Br/Pb ratio is still 75.87/24.13. Both values are almost the same as the one without electron beam irradiation. Similarly, we have also studied the X-ray diffraction (XRD) spectra of lead halide perovskites before and after electron beam irradiation. As shown in Figure 1d, the positions of two main peaks are well preserved at 14.92° and 30.07°.[25] As both of EDS measurement and XRD spectrum relate to the bulk properties, we can conclude that the changes in bulk stoichiometry and crystal structure is very small under low energy electron beam irradiation.

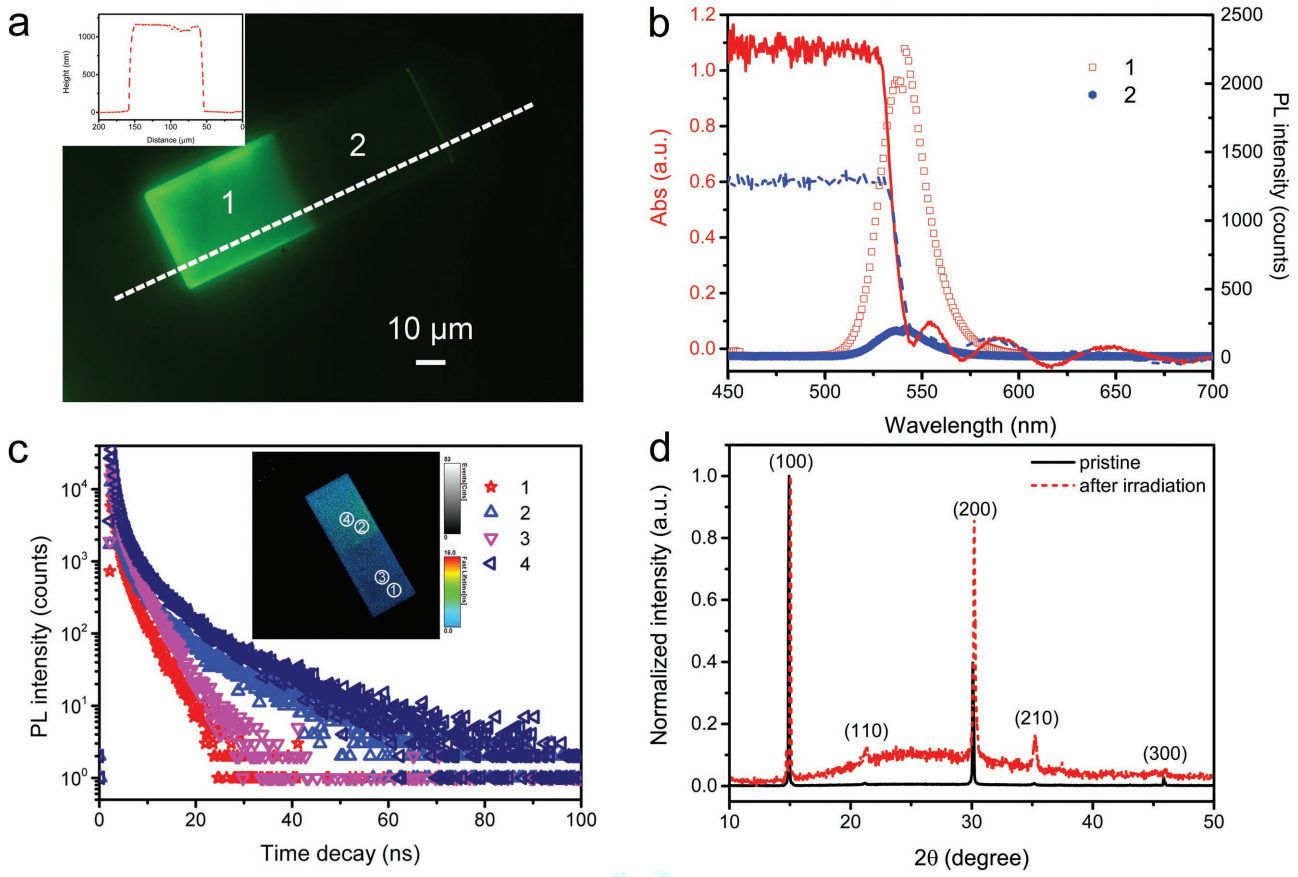

Figure 1. The photoluminescence (PL) and X-ray diffraction (XRD) analysis of $CH_3NH_3PbBr_3$. a) The photoluminescence image of a $CH_3NH_3PbBr_3$ microplate excited by a blue laser. The label of 1 is for the pristine crystal and 2 is for the crystal after exposed to electron beam with a dose of 150 μC cm^{-2} under a voltage of 20 kV. Inset: the thickness analysis of the crystal according to the cut line. b) The absorption (the lines) and photoluminescence (the symbols) spectra at the regions labeled of 1 (red line and red squares) and 2 (blue line and blue circles) in (a). c) The time-resolved decays of photoluminescence in different regions of the microplate under illumination of 485 nm. Inset: the PL lifetime mapping for the microplate. d) XRD spectra relate to the pristine perovskite and the one after irradiation by electron beam with a dose of 150 μC cm^{-2} under a voltage of 20 kV.

To understand the degradation of photoluminescence, we have studied the elementary composition on the surface of lead halide perovskite microplate with X-ray photoelectron spectroscopy (XPS) in **Figure 3**a–e and Figures S5–S7 (Supporting Information). Figure 3a shows the XPS results of the Pb 4f core level in the $CH_3NH_3PbBr_3$ microplate before electron beam irradiation. Two peaks at around 138 and 142.7 eV can be assigned to Pb $4f_{7/2}$ and $4f_{5/2}$, corresponding to the Pb^{2+} in the $CH_3NH_3PbBr_3$ perovskite.[33,34] When the perovskite microplate was irradiated with electron beam, two additional peaks located at around 136 and 140.7 eV can be clearly seen in the investigation for the top surface (Figure 3c) and bottom surface (Figure S7, Supporting Information). These two new peaks correspond to Pb^0 well and indicated the reduction of $Pb^{2\pm}$ at the top and bottom surfaces. Meanwhile, the changes in Br at the surface was also studied. As shown in Figure 3b,d, the relative amount of Br $3d_{5/2}$ around 67.9 eV in Figure 3d is much smaller than the ones in Figure 3b. This kind of reduction can be attributed to the dissociation of Br-Pb bounds and desorption of Br atoms under electron beam irradiation, demonstrated in Figures S5 and S6 (Supporting Information). Similar to Figure 2a, we have periodically irradiated one microplate and scanned the binding energy of 138 eV to obtain the information of Pb^{2+}. The results are shown in Figure 3e. From the emission spectra and the bottom inset, we know that the irradiated regions have weaker photoluminescence. Correspondingly, the periodically weak photoluminescence regions also have much lower Pb^{2+} in the top inset of Figure 3e.

Till now, the consistent experimental results make the effects of low energy electron beam on lead halide perovskites much clear. As the bulk properties of perovskite microplate are well preserved and Pb^0 appear at the surfaces, the radiolysis process should happen during the interaction between low energy electron beam and perovskite. As mentioned above, the electron beam has a good ability of stimulating desorption of bromine atoms and reducing the cations at the top and bottom surfaces. In a reverse way that the passivation of surface states can significantly improve the photoluminescence,[35] here the metallic Pb^0 can greatly enhance the nonradiative process, leading to a significant reduction of photoluminescence intensity. The reduction of Pb^0 has also been confirmed experimentally. As the atomic force microscope (AFM) phase image shown in Figure 3f, a number of circles (with radius of ≈500 nm) can be observed in the regions with electron beam irradiation

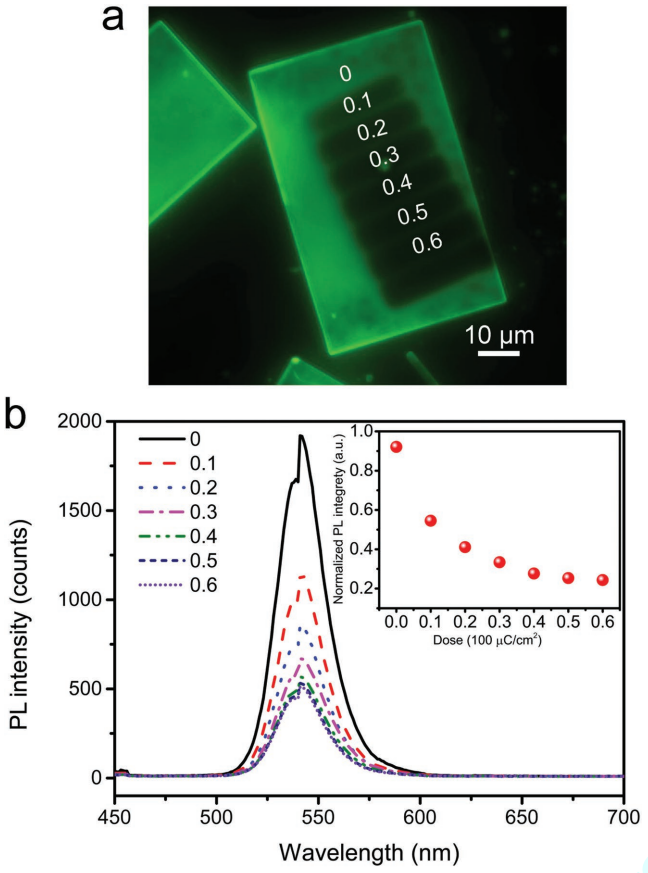

Figure 2. The dependence of photoluminescence on the electron beam dose. a) The photoluminescence image of a perovskite microplate after irradiation with different dose factor of electron beam. The corresponding dose of dose factor from 0 to 0.6 is 0, 15, 30, 45, 60, 75, and 90 μC cm^{-2}, respectively. b) The corresponding photoluminescence spectra vary with the increase of irradiation dose factors. The inset: the integrated output intensity as a function of the dose of electron beam. All the accelerating voltage is 20 kV.

(more results can be seen in Supporting Information). The new phase introduction indicates the formation of new materials after the irradiation by electron beam, also shown in Figure S8 (Supporting Information). Corresponding to the recent reports, these nanoparticles are the aggregation of Pb^0 atoms at the surfaces. This kind of aggregation can be clearly seen from the morphology AFM image in Figures S8c and S9 (Supporting Information). Meanwhile, the crystal structures of the nanoparticles have also been studied by the high resolution TEM measurement. As shown in Figure S10 (Supporting Information), the *d*-spacing of the generated nanoparticles is 0.266 nm, matching the crystal lattice of Pb(101) well. The formation of Pb^0 has been further confirmed with the XRD measurements. By magnifying Figure 1d, the characteristic peak of metallic Pb(101) can be clearly seen at the position around 33.7° (referring to the standard of PDF-2004 in Jade, #44-0872) in Figure S11 (Supporting Information), consistent with the TEM results very well. Even though the energy of electron beam is much lower, we find that the fundamental process of irradiating perovskite with electron beam lithography or even SEM is very similar to the recent TEM experiments (≥80 keV).[27] This finding can significantly increase of possibility of tailoring the perovskite devices with SEM or in typical electron beam writer.

While the electron beam can degrade the photoluminescence, here we would like to show that the electron beam irradiation is not always harmful to the device. We first take the perovskite microlaser as an example to illustrate that the electron beam irradiation can be applied to tailor the performances of lead halide perovskite devices. For a typical rectangle shaped $CH_3NH_3PbBr_3$ microplate, whispering gallery mode (WGM)-based lasers can be simply formed along the well-known diamond orbit. Taking the advantages of high resolution of electron beam, we can selectively irradiate the microplate and modify the internal lasing actions. One example is shown in **Figure 4**a, where 1D periodic strips were generated in the microplate. Then the microplate was optically excited and the lasing properties were studied. When then pumping density was low, a broad photoluminescence has been obtained and the output intensity increased slowly with the increase of pumping density. When the pumping density was above 7.5 μJ cm^{-2}, sharp peaks emerged in the emission spectrum and the output intensity increased dramatically (see inset in Figure 4b). Meanwhile, we have also observed bright spots under the fluorescent microscope (see Figure 4a). Compared with the typical diamond modes in rectangle microplates, here we only observed bright spots at two ends of the periodic strips. The mode spacing in Figure 4b is around 0.5 nm. Following the equation $\Delta\lambda = \lambda^2/2n_gL$, where n_g is the group index, the mode spacing also matches the width of the microplate well. Then we can confirm that the Fabry–Perot lasers instead of WGM lasers have been generated.[36,37] Considering the periodic structure of the microstrips, microlaser array has been successfully formed by the periodically irradiating the microplate with electron beam.

In addition to the 1D microlaser array, the low energy electron beam irradiation can also be used to generate 2D structures. One example is shown in Figure 4c, where filled circles with radius of 500 nm and period of 4 μm have been directly generated with electron beam lithography. When the sample was excited by a frequency doubled Ti:Sapphire laser (400 nm central wavelength, 1 kHz repetition rate, 100 fs pulse duration), the fluorescent microscope image show that the microplate is very close to a green net. While the 2D structure does not give laser emissions, it has the potential in practical applications of micro-LED array. Furthermore, the electron beam irradiation can also be used to generate particular patterns within the perovskite microplate for display. As illustrated in Figure 4d, an image of simplified main building in our university has been directly generated by electron beam lithography. The total size of the logo is around 50 μm, which can be clearly seen under a fluorescent microscope.

Besides the applications in nanopattern generation and microlaser array, the low energy electron beam irradiation can also be applied to improve the performances of optoelectronic devices. Here we will take the perovskite photodetector as an example to illustrate this counterintuitive concept. In typical photodetector, the electron–hole pairs are generated under light illumination. Some of these electron–hole pairs are rapidly separated and collected by the electrodes. Part of them will recombine again and cause some waste of photogenerated carriers. Considering the work function of Pb (≈4.25 eV)

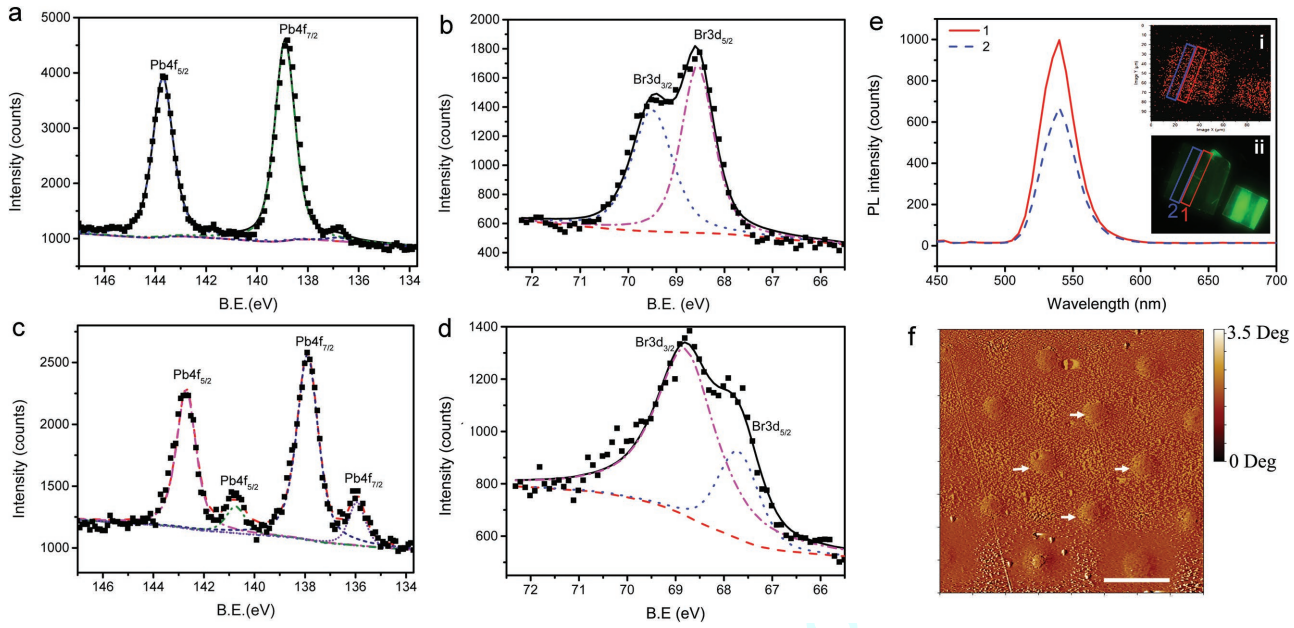

Figure 3. The XPS analysis and AFM measurement of perovskite. a) Pb 4f and b) Br 3d spectra of original $CH_3NH_3PbBr_3$ without irradiation. c) Pb 4f and d) Br 3d spectra of original $CH_3NH_3PbBr_3$ after irradiation with dose of 150 μC cm^{-2} under accelerating voltage of 10 kV. e) The PL spectra in different regions of inset-ii. Inset-i: the XPS mapping of the Pb $4f_{5/2}$ with the binding energy of 138 eV; inset-ii: the PL image of perovskite. The blue box is for the region after irradiation by electron beam with dose of 150 μC cm^{-2} under accelerating voltage of 10 kV and the red one is for the region without irradiation. f) The phase image investigates the surface of perovskite crystal filled circles with radius of 500 nm and period of 4 μm have been directly generated with electron beam lithography by AFM indicated by white arrows. The phase variation indicates some difference of materials, resulting from that different materials have the different modulus. Here the scale bar is 4 μm.

below the conduction band of $CH_3NH_3PbBr_3$ (≈3.4 eV),[38,39] it can function as a good electron collecting layer that collects the electrons quickly and reduce the recombination process.[40] Then Pb as electron collector can efficiently improve the concentration of photogenerated electrons upon excitation. Due to the nature of metal, the propagation loss of electron within these Pb islands can be neglected. In this sense, the Pb islands can bridge different regions and effectively reduce the carrier propagation lengths inside the perovskites. Considering the diffusion lengths of $MAPbBr_3$ are mostly around 10 μm, the formation of Pb layer can significantly reduce the propagation loss of electron and thus increase the photocurrent of perovskite photodetector.

To verify the above analysis, we have experimentally fabricated Au electrodes by standard photolithography and a lift-off process (see details in methods). Then a $CH_3NH_3PbBr_3$ perovskite microplate was transferred onto the electrodes with micromanipulation. **Figure 5**a shows the top-view scanning electron microscope (SEM) image of the device. The separation distances between four electrodes are 10 μm, which are very close to the typical diffusion length. The length and width of the microplate are 51 and 47 μm, respectively. The thickness of the microplate is around 1 μm. By illuminating the photodetector with a LED flash light at 420 nm (intensity of 12 μW cm^{-2}), the purple red squares in Figure 5b show the photocurrent as a function of applied voltage. When the applied voltage was 1 V, the recorded photocurrent was 7.2 nA (normalized current of 3.0 A m^{-2}). Then the sample was irradiated by a 20 kV electron beam with a dose of 400 μC cm^{-2}. After the irradiation, the $CH_3NH_3PbBr_3$ perovskite photodetector was studied with the same conditions again. The corresponding current–voltage (*I*–*V*) characteristic is shown as purple red squares in Figure 5c. When the applied voltage was 1 V, the photocurrent was as large as 15.5 nA (normalized current of 6.5 A m^{-2}). While the light absorption was reduced by electron beam irradiation, the photocurrent density was still enhanced by a factor around 217%. This indicates that the carrier is more efficiently extracted from the lad halide perovskite after the electron beam irradiation, consistent with above analysis well. Interestingly, this enhancement is not limited to particular samples. Similar phenomena have also been in a number of perovskite photodetectors (see details in the Supporting Information). In addition, the response times of the photodetector before and after electron beam irradiation have also been measured. The extracted rise and decay times of irradiated perovskite were 8.3 and 8.3 ms (limited by our instruments and could be faster), which were much smaller than those of pristine perovskite (Figure S12, Supporting Information). These improvements in response times are also consistent with the propagation of electrons through the Pb^0 bridges (islands). Note that the light to dark ratio is not significant here due to the presence of partially continuous Pb^0 layer, which directly contacts the electrodes and increases the dark current. This effect can be eliminated by protecting the regions on electrodes from the electron-beam irradiation.

In summary, the characteristics of lead halide perovskites have been experimentally studied with very low energy electron beam irradiation (accelerating voltage from 5 to 30 keV). From the changes in photoluminescence, EDS measurements, XPS spectrum, and AFM image, we find that a radiolysis process happens and plays an important role in desorption of bromine

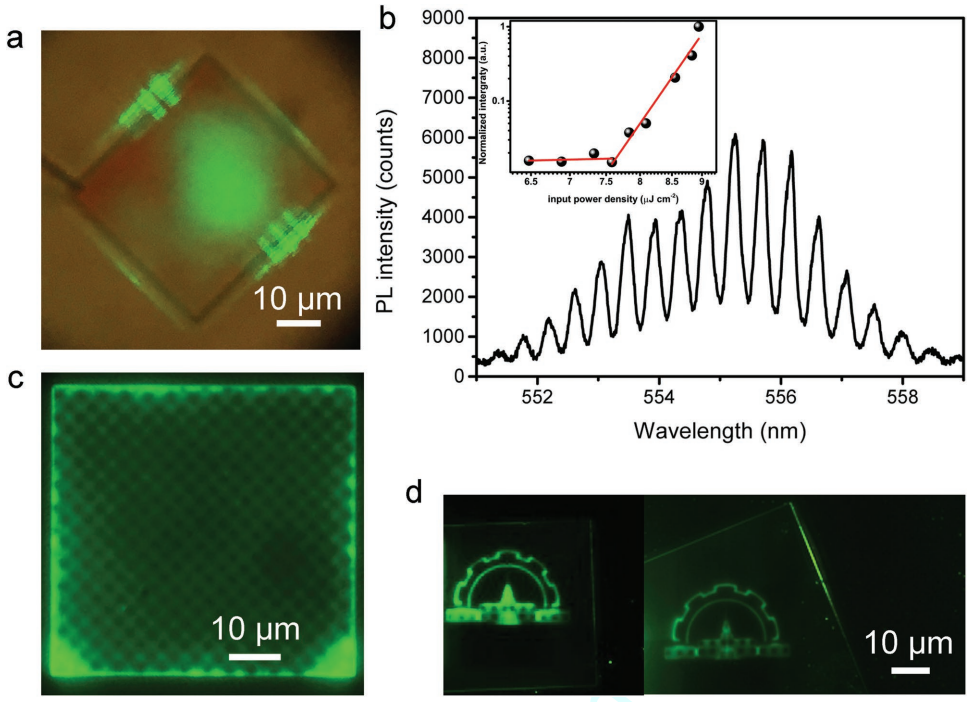

Figure 4. The tailored emission properties of perovskite microplate after electron beam irradiation with a dose of 150 μC cm^{-2} and an accelerating voltage of 10 kV. a) The fluorescent microscope image of a perovskite microplate where 1D grating was directly patterned by electron beam irradiation. Bright spot array can be seen at the side facets. b) The emission spectra of laser arrays in (a) with a pumping density of 30.4 μJ cm^{-2}. Inset: integrated PL intensity as a function of excitation density. c) The fluorescent microscope image of perovskite microplate filled with circles that were directly generated with electron beam lithography. Here the radius of circle is 500 nm and the period is 4 μm. d) An image of simplified main building in our university directly generated by electron beam irradiation.

atoms and reduction of Pb^{2+} to Pb^0 at surfaces. In contrast to the conventional understanding that perovskites are simply degraded, here we show the electron beam irradiation can also be applied to tailor the performances of perovskite optoelectronic devices. With the formation of Pb^0 at top and bottom surfaces, the photoluminescence and corresponding amplification are significantly suppressed. In this sense, periodically patterning a microplate with electron beam lithography, the conventional WGM lasers have been converted to microlaser array. Meanwhile, as the Pb^0 layer can function as a nice carrier conducting layer, the diffusion loss of photon generated carriers within the perovskites shall be reduced. Consequently, the photocurrent of perovskite photodetector after electron beam irradiation has been significantly increased by 217%. This work will route a new way to precisely tailoring or improving the lead halide perovskite devices with typical electron beam lithography.

Experimental Section

Device Fabrication: To fabricate nanostructure devices, 10 nm Ti/40 nm Au electrodes with a separation of 10 μm were first made by photolithography and e-beam evaporation on a 500 nm SiO_2 covered Si wafer. Then a slice of $MAPbBr_3$ crystal was mechanically transferred using a microfiber from the as-grown substrates to the device substrates to cover the electrodes.

Characterization: I–V characteristics were measured with a Keithley 2410 source meter. The devices were illuminated by monochromatic light from a light-emitting diode (450 nm) in the power densities of 2.8, 5.7, and 12 μW cm^{-2}. The responsivity of the response speed was measured using a continuous light (450 nm, 12 μW cm^{-2}) cut off by manual work with an applied voltage of 1 V, and the data were recorded by Keithley 2410 source meter and iPhone. The PL images and spectra were collected from separated multispectral fluorescence microscope (CRi NUANCE EX+) with an excitation wavelength of 450 nm. The time-resolved PL decays were obtained from Nikon A1R confocal integrated system equipped with nikon A1R confocal microscope, detector (2 PMA-Hybrid 40 detectors) and collection controller (TimeHarp260 time correlated single photon counting (TCSPC) unit, version 1.1) in PDL 800-D picosecond pulsed diode laser drived with continous wave (CW) capability (10 MHz, 485 nm). The lifetime was fitted by the software (SymPhoTime 64, version 2.0). The morphology and phase images were measured by the atomic force microscope (CSPM5500, Benyuan Corporation.).The absorption spectra of samples were obtained in a typical home-made optical path and data was collected by fiber optics spectrometer (FLA5000+, FLIGHT Technology Co., Ltd.). XPS was performed with ESCALAB 250Xi (Thermo Fisher), equipped with a monochromatized Al Kα X-ray source (1486.6 eV). Energy calibration was performed fixing the C—C component of C 1s spectrum at 284.8 eV.[33] Relative atomic percentages of different species were computed from high-resolution spectra, fitted with XPSPEAK software. SEM images and EDS analysis of the samples were obtained on a field emission scanning electron microscope (S4700, Hitachi) with an accelerating voltage of 10 kV. The microarrays and gratings were directly written in eLINE Plus (Raith nanofabrication). The laser action was carried with a home-made optical path in Figure S13 (Supporting Information) that an amplified ultrafast laser (1 kHz, 100 fs pulse width) seeded by Ti:Sapphire (Maitai, Spectraphysics) was generated and frequency was doubled by a barium boron oxide (BBO) crystal.

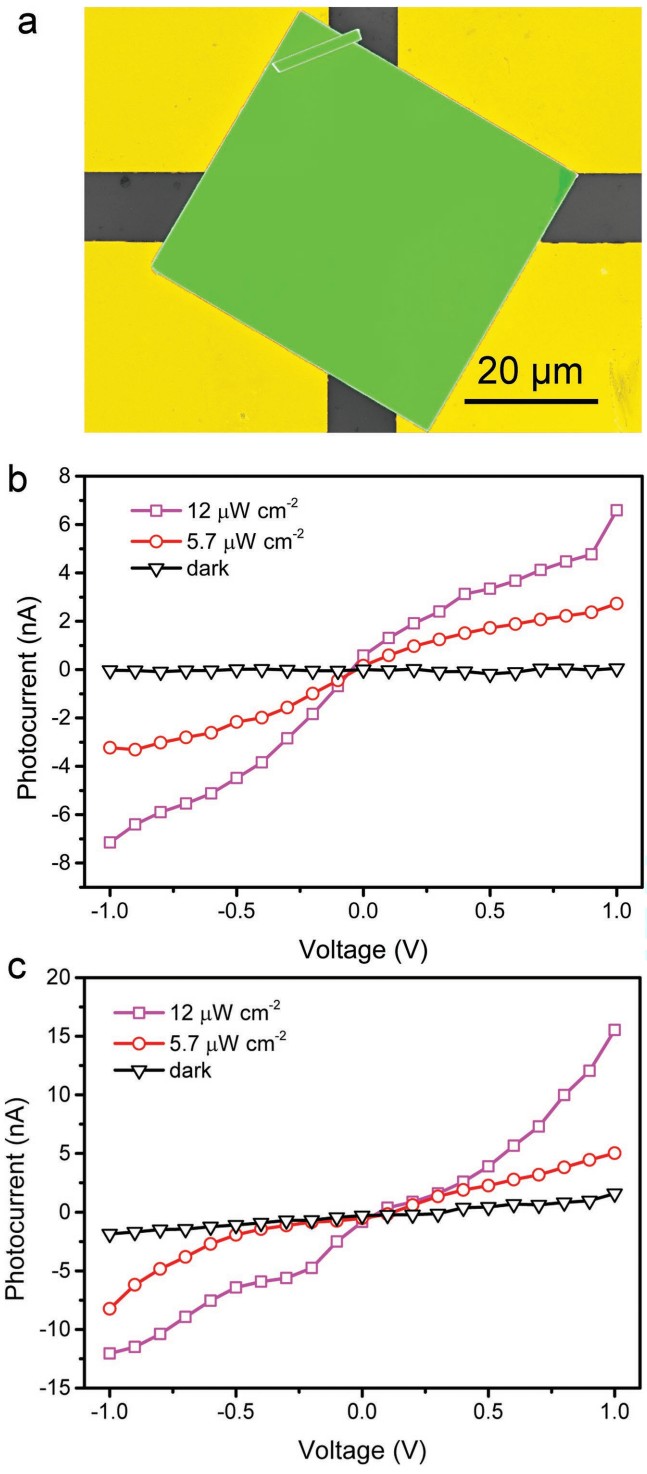

Figure 5. The photoelectric response of a photodetector after electron beam irradiation. a) The top-view SEM image of the device with fake colors. Yellow regions represent the Au electrodes and the green region is the perovskite crystal (≈51 × 47 μm^2). b,c) The recorded photocurrent as a function of applied voltage in the photodetector before (b) and after (c) the electron beam irradiation. Here the dose is 400 μC cm^{-2} and the accelerating voltage is 20 kV. Inset: The transportation of photogenerated electrons in energy band diagram for perovskite photodetector after irradiation by electron beam.

Supporting Information

Supporting Information is available from the Wiley Online Library or from the author.

Acknowledgements

The author would like to thank the financial support from the National Natural Science Foundation of China under the Grant No. 11374078, the Shenzhen Fundamental research projects (JCYJ20160301154309393, JCYJ20160505175637639, and JCYJ20160427183259083), the Public platform for fabrication and detection of micro- and nanosized aerospace devices, and the Shenzhen engineering laboratory on organic–inorganic perovskite devices. The authors thank the MCPC at SUSTech for facility usage and technical support in fluorescence-lifetime imaging microscopy (FLIM) experiments.

Conflict of Interest

The authors declare no conflict of interest.

Keywords

electron-beam irradiation, perovskites, photodetectors

Received: March 23, 2017
Revised: April 26, 2017
Published online:

[1] B. R. Sutherland, H. S. Edward. *Nat. Photonics* **2016**, *10*, 295.
[2] M. A. Green, H. Anita, J. S. Henry, *Nat. Photonics* **2014**, *8*, 506.
[3] S. T. Ha, C. Shen, J. Zhang, Q. H. Xiong, *Nat. Photonics* **2016**, *10*, 115.
[4] T. T. Ngo, S. Isaac, A. Gabriella, C. L. Diego, P. M. P. Juan, M. A. Aurelio, M. S. Ivan, *Adv. Mater.* **2017**, *29*, 1604056.
[5] G. Xing, N. Mathews, S. S. Lim, N. Yantara, X. Liu, D. Sabba, M. Gratzel, S. Mhaisalkar, T. C. Sum, *Nat. Mater.* **2014**. *13*, 476.
[6] J. P. Wang, N. N. Wang, Y. Z. Jin, J. J. Si, Z. K. Tan, H. Du, L. Cheng, X. L. Dai, S. Bai, H. P. He, Z. Z. Ye, M. L. Lai, R. H. Friend, W. Huang, *Adv. Mater.* **2015**, *27*, 2311.
[7] Z. K. Tan, R. S. Moghaddam, M. L. Lai, P. Docampo, R. Higler, F. Deschler, M. Price, A. Sadhanala, L. M. Pazos, D. Credgington, F. Hanusch, T. Bein, H. J. Snaith, R. H. Friend, *Nat. Nanotechnol.* **2014**, *9*, 687.
[8] J. Xing, F. Yan, Y. Zhao, S. Chen, H. K. Yu, Q. Zhang, R. G. Zeng, H. V. Demir, X. W. Sun, A. Huan, Q. H. Xiong, *ACS Nano* **2016**, *10*, 6623.
[9] K. Akihiro, K. Teshima, Y. Shirai, T. Miyasaka, *J. Am. Chem. Soc.* **2009**, *131*, 6050.
[10] W. S. Yang, J. H. Noh, N. J. Jeon, Y. C. Kim, S. Ryu, J. Seo, S. Sang, *Science* **2015**, *348*, 1234.
[11] V. D'Innocenzo, A. R. S. Kandada, M. D. Bastiani, M. Gandini, A. Petrozza, *J. Am. Chem. Soc.* **2014**, *136*, 17730.
[12] A. Amat, E. Mosconi, E. Ronca, C. Quarti, P. Umari, M. K. Nazeeruddin, M. Gratzel, F. D. Angelis, *Nano Lett.* **2014**, *14*, 3608.
[13] B. Conings, L. Baeten, C. D. Dobbelaere, J. D'Haen, J. Manca, H. G. Boyen, *Adv. Mater.* **2014**, *26*, 2041.

[14] N. J. Joen, J. H. Noh, W. S. Yang, Y. C. Kim, S. Ryu, J. Seo, S. Seok, *Nature* **2015**, *517*, 476.
[15] L. T. Dou, Y. M. Yang, J. B. You, Z. R. Hong, W. H. Chang, G. Li, Y. Yang, *Nat. Commun.* **2014**, *5*, 5404.
[16] Y. B. Lee, J. Kwon, E. Hwang, C. H. Ra, W. J. Yoo, J. H. Ahn, J. H. Park, J. H. Cho, *Adv. Mater.* **2015**, *37*, 41.
[17] R. Dong, Y. J. Fang, J. S. Chae, J. Dai, Z. G. Xiao, Q. F. Dong, Y. B. Yuan, A. Centrone, X. C. Zeng, J. S. Huang, *Adv. Mater.* **2015**, *27*, 1912.
[18] S. F. Zhuo, J. F. Zhang, Y. M. Shi, Y. Huang, B. Zhang, *Angew Chem., Int. Ed.* **2015**, *54*, 5693.
[19] J. Z. Song, L. M. Xu, J. H. Li, J. Xue, Y. H. Dong, X. M. Li, H. B. Zeng, *Adv. Mater.* **2014**, *28*, 4861.
[20] Z. G. Xiao, Y. B. Yuan, Y. H. Shao, Q. Wang, Q. F. Dong, C. Bi, P. K. Sharma, A. Gruverman, J. S. Huang, *Nat. Mater.* **2015**, *14*, 193.
[21] Y. B. Yuan, J. S. Huang, *Acc. Chem. Res.* **2016**, *49*, 286.
[22] W. Y. Nie, J. C. Blancon, A. J. Neukirch, K. Appavoo, H. Tsai, M. Chhowalla, M. A. Alam, M. Y. Sfeir, C. Katan, J. Even, S. Tretiak, *Nat. Commun.* **2016**, *7*, 11574.
[23] C. Eames, J. M. Frost, P. R. F. Barnes, B. C. O'regan, A. Walsh, M. S. Islam, *Nat. Commun.* **2015**, *6*, 7497.
[24] O. Hentz, Z. B. Zhao, S. Gradecak, *Nano Lett.* **2016**, *16*, 1485.
[25] N. Zhang, K. Y. Wang, H. H. Wei, Z. Y. Gu, W. Z. Sun, J. K. Li, S. M. Xiao, Q. H. Song, *J. Phys. Chem. Lett.* **2016**, *7*, 3886.
[26] D. W. deQuilettes, W. Zhang, V. M. Burlakov, D. J. Graham, T. Leijtens, A. Osherov, V. Bulovi, H. J. Snaith, D. S. Ginger, S. D. Stranks, *Nat. Commun.* **2016**, *7*, 11683.
[27] Z. Y. Dang, J. Shamsi, F. Palazon, M. Imran, Q. A. Akkerman, S. Park, G. Bertoni, M. Prato, R. Brescia, L. Manna, *ACS Nano* **2017**, *11*, 2124.
[28] J. A. Sichert, Y. Tong, N. Mutz, M. Vollmer, S. Fischer, K. Z. Milowska, R. G. Cortadella, B. Nickel, C. Cardenas-Daw, J. K. Stolarczyk, A. S. Urban, *Nano Lett.* **2015**, *15*, 6521.
[29] L. T. Dou, A. B. Wong, Y. Yu, M. L. Lai, N. Kornienko, S. W. Eaton, A. Fu, C. G. Bischak, J. Ma, T. Ding, N. S. Ginsberg, *Science* **2015**, *349*, 1518.
[30] Y. Yu, D. D. Zhang, C. Kisielowski, L. T. Dou, N. Kornienko, Y. Bekenstein, A. B. Wong, A. P. Alivisatos, P. D. Yang, *Nano Lett.* **2016**, *16*, 7530.
[31] J. Liu, Y. Xue, Z. Wang, Z. Q. Xu, C. Zheng, B. Weber, J. Song, Y. Wang, Y. Lu, Y. Zhang, Q. Bao, *ACS Nano* **2016**, *10*, 3536.
[32] R. F. Egerton, *Microsc. Res. Tech.* **2012**, *7*, 1550.
[33] M. Deepa, F. J. Ramos, S. M. Shivaprasad, S. Ahmad, *Chem. Phys. Chem.* **2016**, *17*, 913.
[34] Q. L. Jiang, M. M. Chen, J. Q. Li, M. C. Wang, X. Q. Zeng, T. Besara, J. L, Y. Xin, X. Shan, B. Pan, C. Wang, *ACS Nano* **2017**, *11*, 1073.
[35] A. H. Ip, S. M. Thon, S. Hoogland, O. Voznyy, D. Zhitomirsky, R. Debnath, L. Levina, L. R. Rollny, G. H. Carey, A. Fischer, K. W. Kemp, *Nat. Nanotechnol.* **2012**, *7*, 577.
[36] K. Wang, W. Sun, J. Li, Z. Gu, S. Xiao, Q. Song, *ACS Photonics* **2016**, *3*, 1125.
[37] W. H. Guo, Y. Z. Huang, Q. Y. Lu, L. J. Yu, *IEEE J. Quantum Electron.* **2003**, *39*, 1563.
[38] H. B. Michaelson, *J. Appl. Phys.* **1977**, *48*, 4729.
[39] Y. C. Ling, Z. Yuan, Y. Tian, X. Wang, J. C. Wang, Y. Xin, K. Hanson, B. W. Ma, H. W. Gao, *Adv. Mater.* **2016**, *28*, 305.
[40] Y. H. Kim, H. Cho, J. H. Heo, T. S. Kim, N. Myoung, C. L. Lee, S. H. Im, T. W. Lee, *Adv. Mater.* **2015**, *27*, 1248.

